

# **Geophysical Research Letters**°



### **RESEARCH LETTER**

10.1029/2023GL106073

### **Key Points:**

- Observations of picket fence spectra differ quantitatively from green aurora spectral observations, suggesting different origins
- Kinetic modeling driven by local parallel electric fields replicates picket fence spectra without requiring particle precipitation
- At 110 km, parallel electric fields between 40 and 70 Townsend (~80–150 mV/m at 110 km) reproduce observed picket fence spectra

#### **Supporting Information:**

Supporting Information may be found in the online version of this article.

#### Correspondence to:

L. C. Gasque, lcgasque@berkeley.edu

### Citation:

Gasque, L. C., Janalizadeh, R., Harding, B. J., Yonker, J. D., & Gillies, D. M. (2023). It's not easy being green: Kinetic modeling of the emission spectrum observed in STEVE's picket fence. *Geophysical Research Letters*, 50, e2023GL106073. https://doi.org/10.1029/2023GL106073

Received 23 AUG 2023 Accepted 24 OCT 2023

### **Author Contributions:**

Conceptualization: L. Claire Gasque, Reza Janalizadeh, Brian J. Harding Data curation: D. Megan Gillies Formal analysis: L. Claire Gasque, Reza Janalizadeh

Investigation: L. Claire Gasque, Reza Janalizadeh, Brian J. Harding Methodology: L. Claire Gasque, Reza Janalizadeh, Brian J. Harding Software: L. Claire Gasque, Brian J. Harding

### © 2023 The Authors.

This is an open access article under the terms of the Creative Commons Attribution-NonCommercial License, which permits use, distribution and reproduction in any medium, provided the original work is properly cited and is not used for commercial purposes.

# It's Not Easy Being Green: Kinetic Modeling of the Emission Spectrum Observed in STEVE's Picket Fence

L. Claire Gasque<sup>1</sup>, Reza Janalizadeh<sup>2</sup>, Brian J. Harding<sup>1</sup>, Justin D. Yonker<sup>3</sup>, and D. Megan Gillies<sup>4</sup>

<sup>1</sup>Space Sciences Laboratory, University of California, Berkeley, Berkeley, CA, USA, <sup>2</sup>Department of Electrical Engineering, The Pennsylvania State University, University Park, PA, USA, <sup>3</sup>Applied Physics Laboratory, The Johns Hopkins University, Laurel, MD, USA, <sup>4</sup>Physics and Astronomy Department, University of Calgary, Calgary, AB, Canada

**Abstract** Recent studies suggest that, despite its aurora-like appearance, the picket fence may not be driven by magnetospheric particle precipitation but instead by local electric fields parallel to Earth's magnetic field. Here, we evaluate the parallel electric fields hypothesis by quantitatively comparing picket fence spectra with the emissions generated in a kinetic model driven by local parallel electric fields energizing ambient electrons in a realistic neutral atmosphere. We find that, at a typical picket fence altitude of 110 km, parallel electric fields between 40 and 70 Td ( $\sim$ 80–150 mV/m at 110 km) energize ambient electrons sufficiently so that, when they collide with neutrals, they reproduce the observed ratio of  $N_2$  first positive to atomic oxygen green line emissions, without producing  $N_2^+$  first negative emissions. These findings establish a quantitative connection between ionospheric electrodynamics and observable picket fence emissions, offering verifiable targets for future models and experiments.

Plain Language Summary The "picket fence" is a captivating visual phenomenon featuring vibrant green streaks often observed with and at lower altitudes than the rare purpleish-white arc called STEVE (Strong Thermal Emission Velocity Enhancement). It occurs in the subauroral sky, at lower latitudes than the auroral oval, raising questions about whether it is a type of aurora or a separate phenomenon. A recent hypothesis proposes that electric fields aligned with Earth's magnetic field in the dense part of the atmosphere where the picket fence forms might energize local electrons, which collide with the neutral atmosphere to create picket fence emissions. This distinguishes the picket fence from traditional auroras caused by energetic particles accelerated higher up in space which stream down and collide with the upper atmosphere. In this study, we compare optical observations of the picket fence to a detailed calculation of the emissions produced by ambient electrons energized by parallel electric fields in the upper atmosphere. The results show that large parallel electric fields can indeed replicate the observed picket fence phenomenon. These findings offer important targets for future picket fence models and experiments. This research demonstrates that the picket fence serves as a valuable testing ground for understanding the chemistry and electrodynamics of Earth's upper atmosphere.

### 1. Introduction: Debate Over the Picket Fence's Origin

STEVE (Strong Thermal Emission Velocity Enhancement) is a rare ionospheric optical phenomenon characterized by a narrow mauve arc extending thousands of kilometers east/west across the subauroral sky (MacDonald et al., 2018). Concurrently with STEVE, vibrant green streaks known as the "picket fence" often appear at lower altitudes after the mauve arc develops and occasionally persist after it fades (Martinis et al., 2022; Nishimura et al., 2023; Yadav et al., 2021). STEVEs are associated with strong sub-auroral ion drifts (SAIDs) (Archer, Gallardo-Lacourt, et al., 2019), but the mechanism behind the optical emissions is still debated (Harding et al., 2020).

Early studies proposed that picket fence emissions, like auroras, are generated by magnetospheric particle precipitation (Bennett & Bourassa, 2021; Chu et al., 2019; MacDonald et al., 2018; Nishimura et al., 2019). Like green aurora, the picket fence primarily consists of 557.7 nm green line (GL) emissions (Gillies et al., 2019). However, the picket fence spectrum published by Gillies et al. (2019) and reanalyzed by Mende et al. (2019) lacks 427.8 nm  $N_2^+$  first negative ( $N_2^+$  1N) emissions, which are ubiquitous and prominent in auroral spectra. The absence cannot be explained by a local  $N_2$  depletion, as Mende et al. (2019) also detect  $N_2$  first positive ( $N_2$  1P) emissions. Instead, Mende et al. (2019) proposed that a local electron population with energies above 7.35 eV but

GASQUE ET AL. 1 of 11



### **Geophysical Research Letters**

10.1029/2023GL106073

Validation: L. Claire Gasque, Reza Janalizadeh, Justin D. Yonker Visualization: L. Claire Gasque Writing – original draft: L. Claire Gasque

Writing – review & editing: L. Claire Gasque, Reza Janalizadeh, Brian J. Harding, Justin D. Yonker, D. Megan below 18.75 eV, could, via collisions with the neutral atmosphere, generate the picket fence emission spectrum. However, they did not quantify how electrons might be locally energized to this energy range.

Recent studies by Lynch et al. (2022) and Mishin and Streltsov (2022) proposed that picket fence emissions arise when low-altitude electric fields parallel to Earth's magnetic field energize local electrons. Lynch et al. (2022) demonstrate that ionospheric conductance gradients created by SAIDs create large field-aligned currents, potentially triggering tearing-mode instabilities similar to those observed in rayed auroral arcs. Mishin and Streltsov (2022) simulated the ionospheric feedback instability (IFI) under SAID conditions. Their approximate solution of the Boltzmann equation indicated that parallel electric fields generated by the IFI might be sufficient to produce the suprathermal electron population responsible for the picket fence emissions. However, neither study conclusively demonstrated whether the electron population energized via their proposed method quantitatively reproduces the observed picket fence spectral features.

In this study, we conduct kinetic calculations to analyze the electron population energized by a parallel electric field in a realistic neutral atmosphere from 100 to 180 km, considering all relevant electron-neutral collisions. Additionally, we compare our calculated spectral features with those in ground-based picket fence observations. Our findings demonstrate that low-altitude parallel electric fields can accelerate local thermal electrons which quantitatively replicate observed picket fence spectra without requiring particle precipitation. Estimating the magnitude of these fields provides a benchmark for future models and observations. This work enables a quantitative comparison between ionospheric electrodynamic models and observable optical emissions, which previous studies have not achieved.

### 2. Picket Fence Spectral Observations

The Transition Region Explorer (TREx) Spectrograph in Lucky Lake, Saskatchewan captures visible (385–801 nm) spectral data for a narrow (~2.1° wide) North/South latitudinal slice of the sky. For additional details about TREx's operation and calibration, refer to Gillies et al. (2019). On 10 April 2018, the same night as the observations presented by Gillies et al. (2019), TREx observed the picket fence several times between 6:28 and 8:00 UT. Figure 1a presents a keogram of the observations, showing the total observed luminosity as a function of elevation angle and time. A full spectrum (385–801 nm) is available at every point. Thin horizontal features brighter than the background are stellar contamination.

Figure 1b displays a keogram of the GL portion of the spectrum (555.2–560.7 nm). Picket fence spectra are identified following the method in Gillies et al. (2019) and Mende et al. (2019). We fit a Gaussian function to the GL luminosity with respect to elevation angle at each time step, determining the elevation angle at the peak brightness  $\mu$  and the standard deviation  $\sigma$ . For luminosity curves with a defined peak at least 200 R above background luminosity, the picket fence spectrum is selected at the elevation bin  $\mu$ , while background spectra are selected at elevation bins  $\pm 3\sigma$  away from  $\mu$ . Picket fence spectra with stellar contamination are discarded, and contaminated background spectra are replaced by neighboring uncontaminated pixels. Figure 1c displays the extracted picket fence spectra (black dots) and the selected poleward (blue triangles pointing up) and equatorward (red triangles pointing down) backgrounds between 6:49 and 7:00 UT.

The picket fence is expected to lie between 97 and 150 km and be approximately aligned with the magnetic field (Archer, St.-Maurice, et al., 2019; Semeter et al., 2020). The black dotted line in Figure 1d represents the look direction up the magnetic field, calculated using the International Geomagnetic Reference Field, Version 13 (IGRF13) (Michael, 2021; Wardinski et al., 2020). Our kinetic model described in Section 3 assumes emissions originate from a uniform source at a single altitude, avoiding assumptions about the vertical parallel electric field profile. Consequently, we select picket fence spectra closer to the horizon, away from the magnetic field look direction, to reduce the vertical profile intersected by the line-of-sight. Specifically, we use 45 uncontaminated picket fence spectra observed between 6:45 and 7:30 UT, all with elevation angles between 131° and 142°. Figure 1d depicts the picket fence observation geometry at 6:52 UT. The observed GL luminosity is projected onto an arc (shown as a green line arbitrarily depicted at 200 km for illustration purposes), and the equatorward and poleward picket fence boundaries are marked by solid red and blue lines, respectively. The observed picket must lie within the wedge formed by these boundaries, as illustrated by the green rectangle in the figure. Assuming that the picket fences are 5–25 km wide latitudinally (Liang, Zou, et al., 2021), we estimate that the line-of-sight cuts through no more than 25 km of the altitudinal profile for the selected observations, with most

GASQUE ET AL. 2 of 11

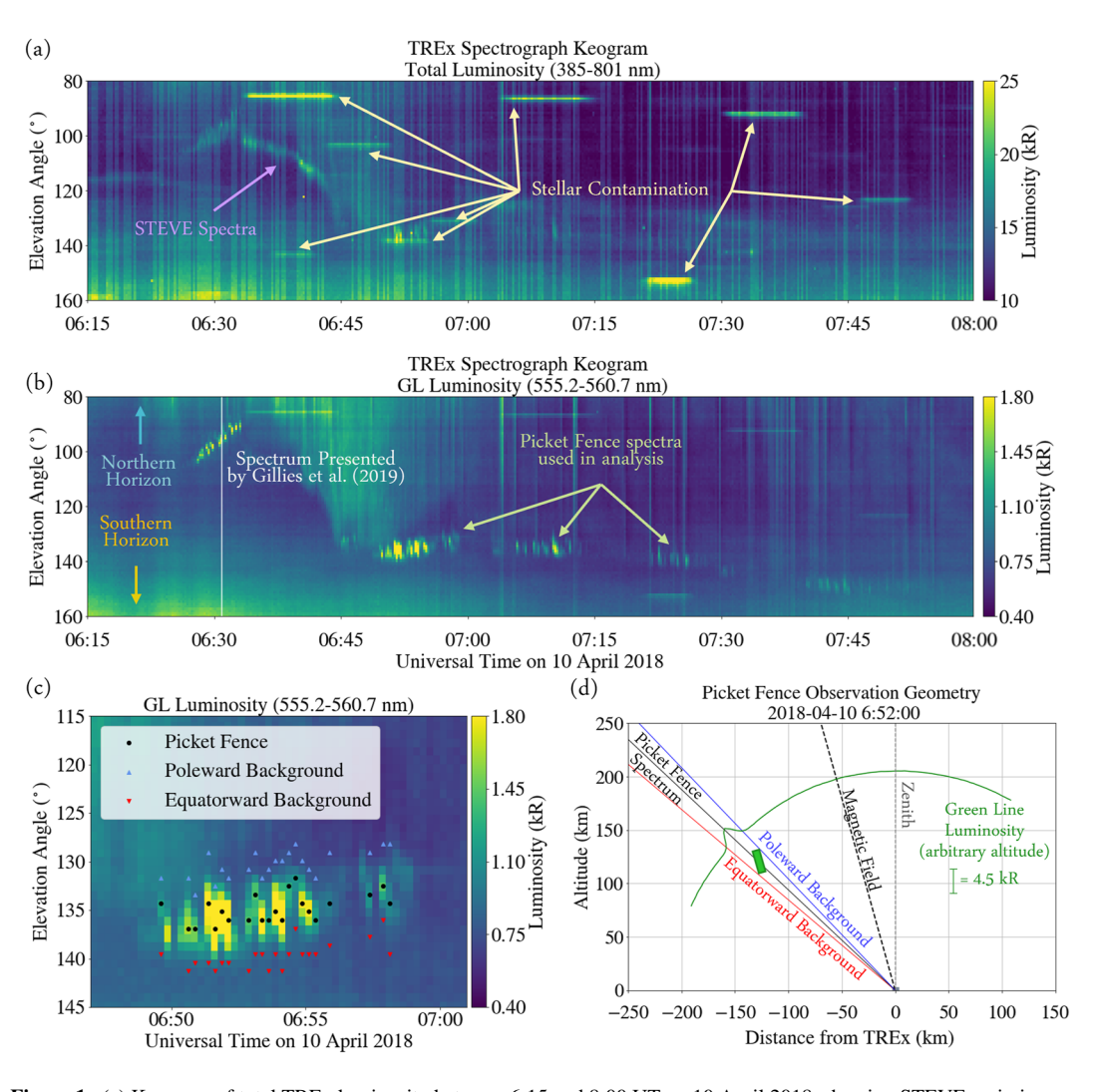


**Figure 1.** (a) Keogram of total TREx luminosity between 6:15 and 8:00 UT on 10 April 2018, showing STEVE emissions and stellar contamination. A full spectrum (385–801 nm) is available at every point. (b) Keogram of TREx GL observations (555.2–560.7 nm) during the same period, highlighting the picket fence observations. (c) Picket fence and background spectra extracted between 6:49 and 7:00 UT. Some spectra were removed due to stellar contamination. See text for details of selection process. (d) Approximate observation geometry for picket fence observed at 6:52 UT. The sample picket shown is only a representation as the altitude of the emissions is unknown.

examples cutting through no more than 15 km. Due to these observational constraints, our quantitative results in Section 4 represent vertical averages over a maximum of 25 km.

We isolate individual picket fence spectra by subtracting the average of their poleward and equatorward background spectra. The error in each spectrum is determined by propagating the standard deviation variations in the background spectra at each wavelength through the background subtraction. We compute median luminosities from the 45 picket fence spectra at each wavelength (Figure 2a), repeating the procedure for the background-subtracted spectra (Figure 2b). The dominant features are the 557.7 nm GL and the  $N_2$  1P band system, while the 427.8 nm  $N_2^+$  1N emissions observed in the background spectra are absent in the picket fence spectrum, consistent with the findings of Mende et al. (2019).

Instead of directly comparing the absolute observed brightness to our model results, which requires assuming the picket fence's latitudinal width and the local electron density, we focus on comparing the ratio of  $N_2$  1P and GL luminosities. For the GL, we calculate the luminosity between 555.2 and 560.7 nm, accounting for the GL's spectral width. For  $N_2$  1P, we calculate the luminosity between 642 and 700 nm. Although  $N_2$  1P emissions extend to infrared (IR) wavelengths and TREx's range extends to 800 nm, we only consider this part of the spectrum to

GASQUE ET AL. 3 of 11

19448007, 2023, 21, Downloaded from https://agupubs.onlinelibrary.wiley.com/doi/10.1029/2023GL106073 by Pennsylvania State University, Wiley Online Library on [09/11/2023]. See the Terms

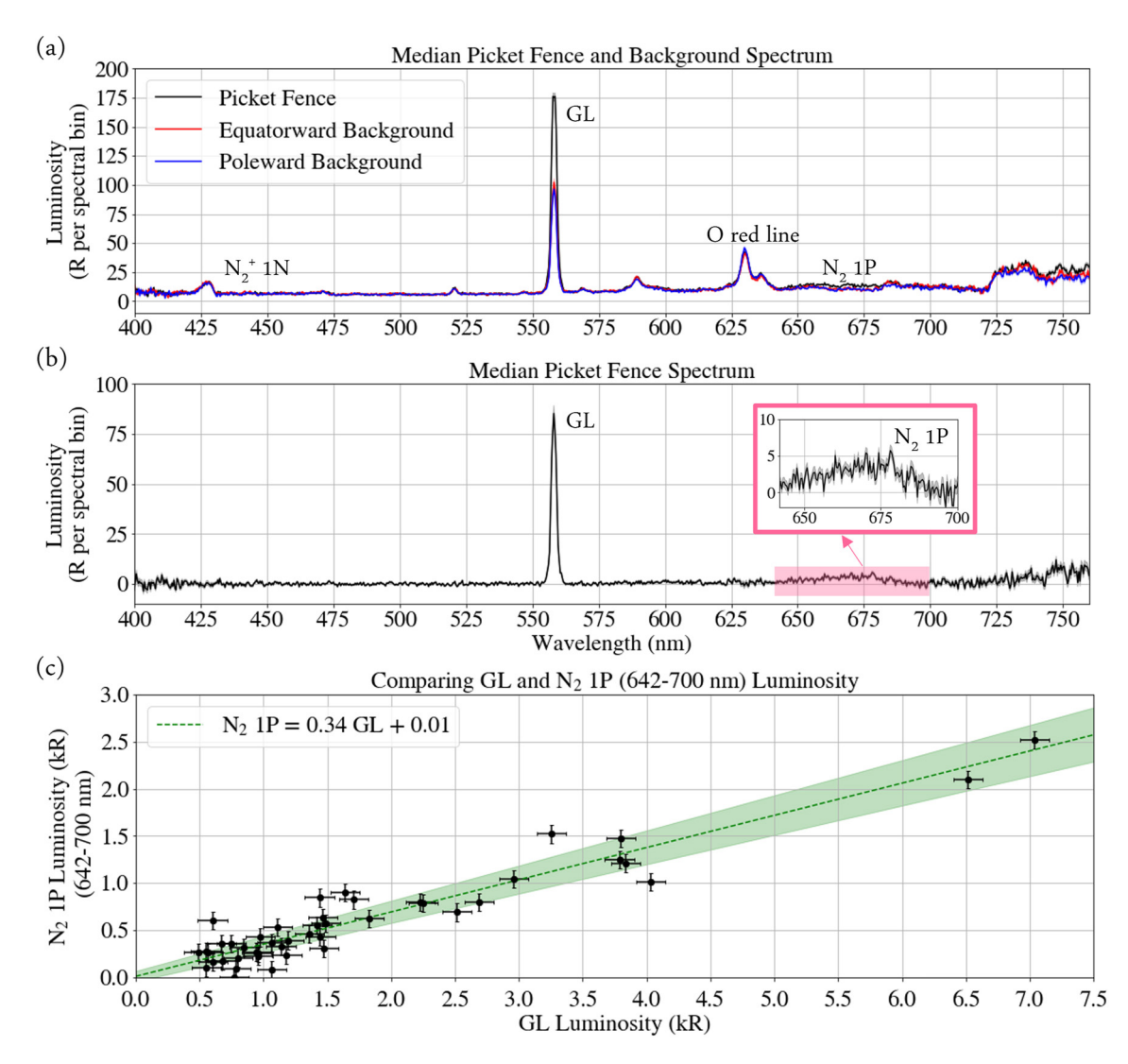


**Figure 2.** (a) Median picket fence spectrum (black) and poleward (blue) and equatorward (red) background spectra. (b) Median picket fence spectrum after background subtraction. Inset: N<sub>2</sub> 1P spectrum (642–700 nm). (c) Ratio of N<sub>2</sub> 1P (642–700 nm) to GL luminosity from the TREx observations, scaled to account for atmospheric transmission.

avoid larger errors near the edge of TREx's observational band and complications from  $O_2$  atmospheric absorption above 700 nm

To quantitatively compare the in situ ratio of  $N_2$  1P to GL emissions, we must consider atmospheric transmission between the emission source and TREx. We apply an atmospheric transmission profile from Figure 1a of Morrill et al. (1998), which corresponds to a source at 65 km observed from the ground at an elevation angle of  $40^\circ$ , similar to our observations. While the picket fence occurs at higher altitudes, most atmospheric scattering and absorption occurs in the lower atmosphere, so this difference is assumed to be negligible (Meier, 1991). According to Morrill et al. (1998), the transmittance at 557.7 nm for GL is 0.42, and the average transmittance for  $N_2$  1P between 642 and 700 nm is 0.53. This results in a transmittance ratio of  $\sim$ 1.26 between the two features.

We perform linear regression on the data using the model  $y = \alpha x + \beta$ , where y represents the N<sub>2</sub> 1P luminosities, x represents the GL luminosities,  $\alpha$  represents the luminosity ratio, and  $\beta$  represents the intercept. We estimate the best fit parameters and their errors following the method described by Gull (1989), applying Bayesian statistics to linear regression with errors in both variables. Our analysis yields  $\alpha = 0.34 \pm 0.03$  and  $\beta = 9.4 \pm 56.9$  R. These results are displayed in Figure 2c. Mende et al. (2019) conducted a similar analysis without considering transmission effects and found an N<sub>2</sub> 1P to GL ratio of 0.39. If we neglect transmission effects, our ratio is  $\alpha = 0.43 \pm 0.04$ , which is consistent with Mende et al. (2019)'s findings. We emphasize that the ratio for green

GASQUE ET AL. 4 of 11

19448007, 2023, 21, Downloaded from https://agupubs.onlinelibrary.wiley.com/doi/10.1029/2023GL106073 by Pennsylvania State University, Wiley Online Library on [09/11/2023]. See the Terms

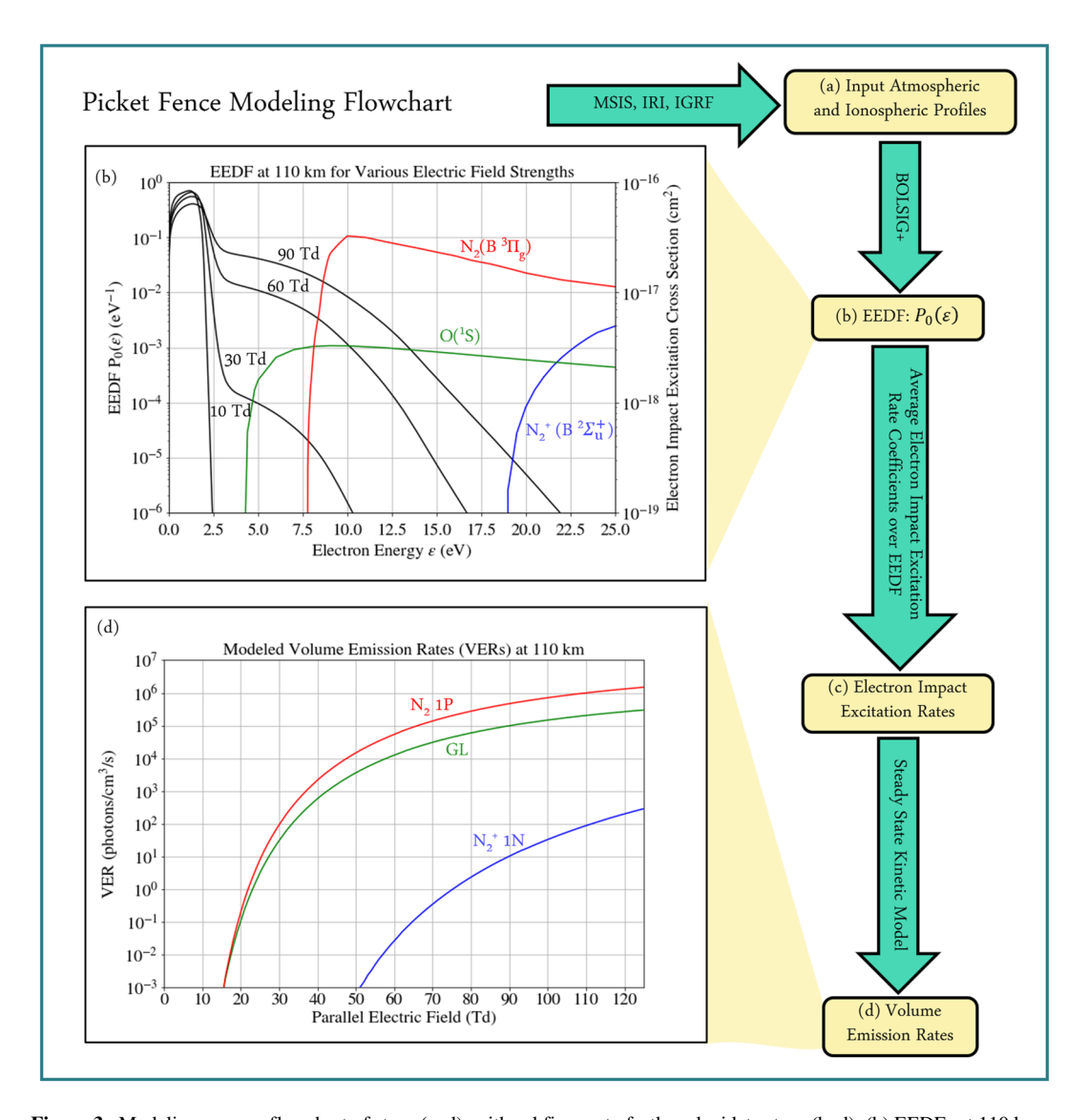


Figure 3. Modeling process flowchart of steps (a–d), with subfigures to further elucidate steps (b, d). (b) EEDFs at 110 km for different parallel electric field strengths, overlaid with electron impact excitation cross sections for  $O(^1S)$ ,  $N_2(B^3\Pi_g)$ , and  $N_2^+(B^2\Sigma_u^+)$ . (d) VERs at 110 km for GL,  $N_2$  1P, and  $N_2^+$  1N calculated with the steady state kinetic model.

aurora is 0.72 (Vallance Jones, 1974), significantly different from our picket fence results. This observation reinforces that the picket fence and green aurora are likely generated by different mechanisms.

### 3. Kinetic Modeling of Emissions Driven by Parallel Electric Fields

Successful models of mechanisms generating the picket fence must be able to achieve the observed ratio of 0.34 between  $N_2$  1P (642–700 nm) and GL emissions while keeping  $N_2^+$  1N emissions undetectable. Here, we explore whether a kinetic model driven solely by parallel electric fields can replicate these features. The following subsections outline the modeling process, including determining the atmospheric and ionospheric inputs, analyzing the effect of a parallel electric field on the local electron energy distribution function (EEDF), and employing steady-state kinetic modeling to calculate volume emission rates (VERs) of excited atomic and molecular states. Figure 3 summarizes the modeling process.

### 3.1. Model Inputs: Atmospheric and Ionospheric Conditions

We use established models to characterize atmospheric, ionospheric, and magnetic field conditions for the time, location, and geomagnetic conditions of the TREx observations described in Section 2. The Naval Research

GASQUE ET AL. 5 of 11

Laboratory's Mass Spectrometer Incoherent Scatter Radar (MSIS) model version 2.1 provided profiles of neutral temperature and densities for eight neutral species (Emmert et al., 2021, 2022; Lucas, 2023; Picone et al., 2002). Ionospheric electron density and temperature profiles were taken from the International Reference Ionosphere 2016 (IRI16) (Bilitza et al., 2017; Ilma, 2017). The magnitude of the magnetic field was obtained from IGRF13 (Michael, 2021; Wardinski et al., 2020). The resulting profiles are shown in Figure S1 of Supporting Information S1.

Using these profiles assumes that picket fence conditions are similar to climatological conditions. However, STEVE and the picket fence are associated with intense SAIDs (Archer, Gallardo-Lacourt, et al., 2019; MacDonald et al., 2018), rare events characterized by narrow channels of hot, fast-flowing, and depleted plasma (Liang, St-Maurice, & Donovan, 2021). Although IRI does not replicate these conditions, the ratio between  $N_2$  1P (642–700 nm) and GL emissions is independent of electron density (see Text S1 of Supporting Information S1), so this does not affect our results. Additionally, Mishin and Streltsov (2022) suggested that SAID conditions may lead to neutral upwelling, which is not captured by MSIS and which may decrease the  $O/N_2$  ratio at picket fence altitudes. Doubling the  $O/N_2$  ratio input in our model introduces changes on the order of 25% to our electric field magnitude predictions which, while significant, do not alter our qualitative findings.

### 3.2. Calculating EEDFs and Electron Impact Excitation Rates

We used BOLSIG+ (version 12/2019) (Hagelaar & Pitchford, 2005) to solve the Boltzmann equation, quantifying changes in the EEDF with altitude and parallel electric field strength. BOLSIG+ calculates a steady-state solution under a uniform electric field, accounting for the effects of electron-neutral collisions in a user-defined atmosphere. Time-dynamics, non-local electron transport, and electric field gradients are not considered, and we neglect the effect of Coulomb collisions (Gurevich, 1978). For additional details about BOLSIG+, see Hagelaar and Pitchford (2005). Fractional densities of  $N_2$ ,  $O_2$ , and O were obtained from MSIS. Electron impact collisional cross sections of  $N_2$ ,  $O_2$ , as packaged with the BOLSIG+ software, were obtained from the LXCat Database (Pancheshnyi et al., 2012) based on data published by Phelps and Pitchford (1985) and Lawton and Phelps (1978), respectively. We added the O cross sections, obtained from Laher and Gilmore (1990), to BOLSIG+.

We consider altitudes between 100 and 180 km, where the 180 km upper bound is well above the expected picket fence altitude (Archer, St.-Maurice, et al., 2019). The 100 km lower bound approximately marks the division between the atmospheric collisional regime, where collisions among excited states are important, and the radiational regime dominated by electron impact excitation (Yonker & Bailey, 2020). We considered reduced parallel electric fields ranging from E/N = 0 to 120 Townsend (Td) where E is the electric field in V/m, N is the neutral density in m<sup>-3</sup>, and 1 Td =  $10^{-21}$  V m<sup>2</sup>. The upper limit corresponds to the breakdown field  $E_k$  in conventional air at low altitudes (Raizer, 1991, p. 137).

Figure 3b displays EEDFs at 110 km for parallel electric fields of 10, 30, 60, and 90 Td (equivalent to 20, 60, 115, and 170 mV/m at 110 km, respectively). The figure highlights several electron impact collisional cross sections:  $O({}^{1}S)$  in green,  $N_{2}(B^{3}\Pi_{g})$  in red, and  $N_{2}^{+}(B^{2}\Sigma_{u}^{+})$  in blue. Stronger electric fields stretch the tail of the EEDF to higher energies, enhancing high-energy electron populations and increasing electron impact excitation rate coefficients.

### 3.3. Calculating Volume Emission Rates

To calculate theoretical VERs for  $N_2$  1P, GL, and  $N_2^+$  1N emissions, we implement a steady-state kinetic model which accounts for additional production and loss processes for excited states of  $N_2$  and O. For  $N_2$  1P emissions, produced through relaxation of the  $N_2(B^3\Pi_g)$  state to the  $N_2(A^3\Sigma_u^+)$  state, we account for radiative cascade from higher  $N_2$  triplet states (Meier, 1991). For GL emissions, produced via relaxation of the  $O(^1S)$  state to the  $O(^1D)$  state, we incorporate additional  $O(^1S)$  production via O quenching of  $N_2(A^3\Sigma_u^+)$ . We also consider additional quenching of  $O(^1S)$  and  $N_2(A^3\Sigma_u^+)$  by O,  $O_2$ , and NO.  $N_2^+$  1N emissions occur via relaxation of  $N_2^+(B^2\Sigma_u^+)$  state to the ground state of  $N_2^+$  following electron impact ionization (Shemansky & Liu, 2005). For more details about these calculations, see Text S1 in Supporting Information S1.

We compared these calculated VERs to those obtained by inputting our electron impact excitation rates into Yonker and Bailey (2020)'s model, which includes interactions between individual  $N_2$  excited states and resolves

GASQUE ET AL. 6 of 11

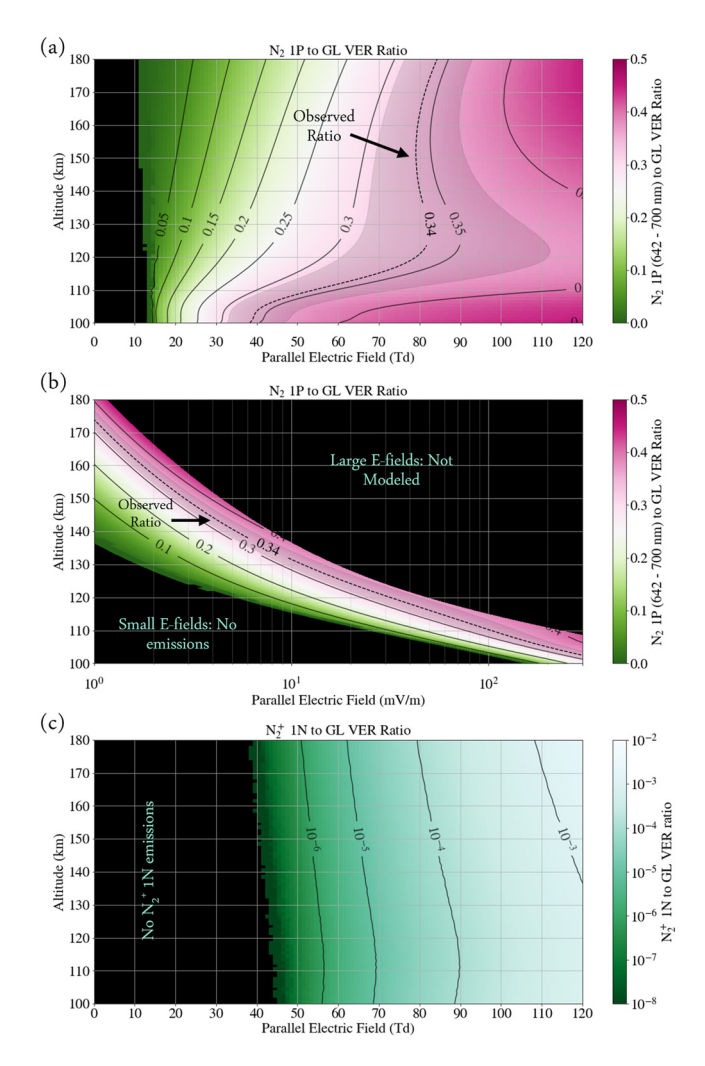


**Figure 4.** (a) Calculated  $N_2$  1P (642–700 nm) to GL VER ratios. Observed luminosity ratios and margins of error are indicated by the black dotted line and shaded region, respectively. (b) The same as (a), but with parallel electric field strength in mV/m. (c) Calculated  $N_2^+$  1N (421–431 nm) to GL VER ratios.

the vibrational states of  $N_2$ . Between 105 and 150 km, the difference in the  $N_2$  1P to GL emission ratio between our model and Yonker and Bailey (2020)'s is below 15%, demonstrating excellent agreement. At lower altitudes, where the collisional regime dominates, the difference remains below 40%.

Figure 3d presents the modeled VERs for  $N_2$  1P, GL, and  $N_2^+$  1N at 110 km as a function of parallel electric field strength. The VERs are directly proportional to electron density, which may be depleted under SAID conditions, so the actual VERs may be reduced if the picket fence lies within the depleted channel. However, the ratio between these VERs remains independent of the electron density.

### 4. Comparison With Observations

Figures 4a and 4b present calculated  $\rm N_2$  1P to GL VER ratios for parallel electric fields in units of Td and mV/m, respectively, where the  $\rm N_2$  1P spectrum has been truncated to only include the 642–700 nm portion. The IR picket fence  $\rm N_2$  1P spectrum has never been measured, so we use an estimated scaling factor of ~8% determined from modeling of the  $\rm N_2$  1P spectrum in aurora, presented in Table 4.12 of Vallance Jones (1974). The observed ratio and its data-driven uncertainty are indicated in Figures 4a and 4b by the black dotted lines and shaded regions, respectively. At 110 km, the observed  $\rm N_2$  1P (642–700 nm) to GL ratio is reproduced for parallel electric field strengths between 40 and 70 Td (~80–150 mV/m at 110 km). Assuming a picket fence width of ~10 km, a uniform emission source, and electron densities given by IRI, this corresponds to GL luminosities between 0.5 and 31 kR, consistent with observations.

If the  $N_2$  ( $B^3\Pi_g$ ) vibrational distribution differs between aurora and the picket fence, the shape of the  $N_2$  1P spectrum may also differ. A test was performed in which our electron impact excitation rates were inputs to Yonker's vibrationally resolved model; the results suggested the 642–700 nm portion may account for 12%–14% of the total  $N_2$  1P spectrum. Adopting this higher scale factor leads to a ~50% reduction in our predicted parallel electric field strength at 110 km. Obtaining a picket fence  $N_2$  1P spectrum extending into the IR would enhance confidence in our quantitative estimates of parallel electric field strength, although our qualitative findings remain unchanged.

The calculated  $N_2^+$  1N to GL VER ratios are presented in Figure 4c. Even for large parallel electric field strengths, this ratio remains below  $10^{-3}$  at picket

fence altitudes, undetectable by the TREx spectrograph for even the brightest picket fence events. Thus, we find that parallel electric fields of realistic magnitudes will not produce observable  $N_2^+$  1N emissions.

These results demonstrate that a model driven by parallel electric fields can reproduce all of the key picket fence spectral features at picket fence altitudes, strongly supporting local parallel electric fields as a plausible driving mechanism for picket fence emissions.

### 5. Discussion and Conclusion

This study provides quantitative evidence that spectral features of picket fence emissions can be reproduced by a kinetic model driven solely by local parallel electric fields, offering a substantiated alternative to magnetospheric precipitation, which lacks supporting spectral evidence. As a reference point for future observations and modeling, we find that at 110 km 40–70 Td (~80–150 mV/m at 110 km) parallel electric fields produce observationally consistent picket fence spectra. The developed kinetic and chemical modeling tools could be used as post-processors or two-way coupled into global or regional MHD models to simulate the picket fence or its potential connections to other subauroral phenomena such as SAIDs, STEVE, or stable auroral red (SAR) arcs

GASQUE ET AL. 7 of 11

(Gallardo-Lacourt et al., 2021; Gillies et al., 2023; Harding et al., 2020; Liang, St-Maurice, & Donovan, 2021; Martinis et al., 2022).

While we have demonstrated the plausibility of parallel electric fields as a driving mechanism for the picket fence, further measurements are essential to validate or challenge this hypothesis. Our modeling demonstrates that parallel electric fields of magnitudes considered here would not generate observable  $N_2^+$  1N emissions. Therefore, any future observations of  $N_2^+$  1N emissions in a picket fence would prompt reassessment of this mechanism. Furthermore, Text S2 in Supporting Information S1 describes an extension of our model to predict ultraviolet (UV) spectral features of the picket fence, which could be confirmed by space-based observations. For the brightest picket fence events, we find that  $N_2$  Vegard-Kaplan (VK), Lyman-Birge-Hopfield (LBH), and  $N_2$  Second Positive emissions could be promising observational targets. However, 1356 Å atomic oxygen emissions are unlikely to be observable, as shown in Figure S2 in Supporting Information S1. Additionally, expanding this analysis to include more picket fence spectra would help capture the true extent of the variability in these spectra and further assess the consistency with the parallel electric field driving mechanism.

If parallel electric fields indeed drive picket fence emissions, the structure of the picket fence constrains the electric field's structure. Under the influence of a parallel electric field at picket fence altitudes, the EEDF equilibrates in between  $\sim$ 0.1 and 50 ms, increasing with altitude (Gurevich, 1978). Given the  $\sim$ 0.7 s radiative lifetime of  $O(^1S)$  (Itikawa & Ichimura, 1990), and the several microseconds radiative lifetime of  $N_2(B^3\Pi_g)$  (Eyler & Pipkin, 1983), visible emissions should emerge within 1 s of the parallel electric field onset, depending on the altitude. While electron transport or neutral winds may induce some blurring, the emissions should predominantly trace the parallel electric fields. As a result, the electric fields would exhibit similar structure to the picket fence itself: aligned in a rayed east/west arc, confined between 97 and 150 km in altitude, and organized along the local magnetic field (Archer, St.-Maurice, et al., 2019). However, the non-field-aligned emission "streaks" below the picket fence (103–108 km) may not trace parallel electric fields, as these are hypothesized to be a consequence of plasma turbulence (Semeter et al., 2020).

While this study refrains from speculating on sources or resulting altitude profiles of parallel electric fields, Lynch et al. (2022) and Mishin and Streltsov (2022) suggest that parallel electric fields could be the consequence of different ionospheric instabilities driven by extreme SAIDs. Lynch et al. (2022) suggest that wave electric fields parallel to the magnetic field, arising from a tearing-mode instability, could drive the picket fence. Although they do not model the magnitude or frequency of these waves, our study's results are applicable to wave electric fields which vary significantly slower than the EEDF equilibration timescale. Mishin and Streltsov (2022)'s simulation of the ionospheric feedback instability yielded maximum field strengths of  $\sim$ 26 mV/m, occurring at 130–140 km. Our predictions achieved the observed  $N_2$  1P to GL emissions ratio for  $\sim$ 7 mV/m electric field strengths at 135 km, showing reasonable agreement with Mishin and Streltsov (2022)'s results.

Local parallel electric fields may play a significant role in the ionosphere beyond the picket fence. In the auroral region, certain optical features share spectral characteristics with the picket fence and cannot be explained by precipitation. Fragmented aurora-like emissions (FAE) are non-field aligned green patches showing GL and  $N_2$  1P emissions but lacking  $N_2^+$  1N (Dreyer et al., 2021). Enhanced aurora (EA) consist of thin, bright layers within regular aurora, exhibiting increased  $N_2$  1P relative to  $N_2^+$  1N (Hallinan et al., 1997). Similar to the picket fence, both FAE and EA are suggested to result from suprathermal electron populations locally generated by parallel electric fields or wave-particle interactions (Dreyer et al., 2021; Hallinan et al., 1997). Karlsson et al. (2005) simulated EA using a simple auroral current model, generating parallel electric fields with maximum strength of ~30 mV/m peaking between 80 and 120 km. Collectively, this suggests that the picket fence might represent one example of a class of aurora-like emissions generated locally by parallel electric fields, not magnetospheric particle precipitation, although the sources of these fields may differ. These findings underscore the potential significance of local parallel electric fields. In particular, since visible and ultraviolet auroral observations are increasingly used to trace particle precipitation and infer magnetospheric activity, it is important to better understand and quantify other sources of emission beyond particle precipitation. Thus, investigating the prevalence and sources of these parallel electric fields warrants further attention from the broader scientific community.

The most definitive way to verify the existence of these parallel electric fields is with in situ measurements. While magnetospheric parallel electric fields have long been associated with auroral particle acceleration and precipitation (Marklund, 1993; Paschmann et al., 2003; Shelley, 1995), static current closure models predict parallel electric fields from the ionospheric F-region to the E-region to be orders of magnitude weaker than perpendicular

GASQUE ET AL. 8 of 11

19448007, 2023, 21, Downloaded

Acknowledgments

We express our gratitude to Stephen

this study. We also acknowledge the

University of Colorado Space Weather

Technology, Research and Education

Center for providing pyMSIS. Partial

support for this work was provided by

NSF Grant AGS-2010088 to Pennsyl-

vania State University, NASA Grant

80NSSC21K1386 to the University

of California, Berkeley, and the

Robert P. Lin Fellowship.

Mende and John Bonnell for their

inspiration and valuable input in

fields ( $\mu$ V/m rather than mV/m) (e.g., Farley Jr, 1959). Ionospheric electric field measurements routinely assume zero parallel electric field when deriving a full vector perpendicular field from two-dimensional measurements (Pfaff et al., 2021). However, satellite measurements of enhanced downward currents and modeling of the ionospheric response suggest significant parallel fields in the collisional base of the D and E regions (Karlsson & Marklund, 1998; Marklund et al., 1997), but to our knowledge, no measurements have probed the existence of these fields. Confirming the existence of these fields is crucial for advancing our understanding of a wide variety of phenomena in the auroral and subauroral regions. Based on our study's results, we propose that attempting to measure these electric fields in situ should be a priority for the space physics community.

### **Data Availability Statement**

The Transition Region Explorer Spectrograph (TREx Spectrograph) is a joint Canada Foundation for Innovation and Canadian Space Agency project developed by the University of Calgary. The TREx data used in this study is available freely (Gillies, 2023).

### References

- Archer, W., Gallardo-Lacourt, B., Perry, G. W., St.-Maurice, J.-P., Buchert, S. C., & Donovan, E. (2019). Steve: The optical signature of intense subauroral ion drifts. *Geophysical Research Letters*, 46(12), 6279–6286. https://doi.org/10.1029/2019gl082687
- Archer, W., St.-Maurice, J.-P., Gallardo-Lacourt, B., Perry, G., Cully, C., Donovan, E., et al. (2019). The vertical distribution of the optical emissions of a Steve and Picket Fence event. *Geophysical Research Letters*, 46(19), 10719–10725. https://doi.org/10.1029/2019gl084473
- Bennett, C. L., & Bourassa, N. (2021). Improved analysis of STEVE photographs. *Journal of Geophysical Research: Space Physics*, 126(4), e2020JA027843. https://doi.org/10.1029/2020ja027843
- Bilitza, D., Altadill, D., Truhlik, V., Shubin, V., Galkin, I., Reinisch, B., & Huang, X. (2017). International reference ionosphere 2016: From ionospheric climate to real-time weather predictions. *Space Weather*, 15(2), 418–429. https://doi.org/10.1002/2016sw001593
- Chu, X., Malaspina, D., Gallardo-Lacourt, B., Liang, J., Andersson, L., Ma, Q., et al. (2019). Identifying STEVE's magnetospheric driver using conjugate observations in the magnetosphere and on the ground. *Geophysical Research Letters*, 46(22), 12665–12674. https://doi.org/10.1029/2019gl082789
- Dreyer, J., Partamies, N., Whiter, D., Ellingsen, P. G., Baddeley, L., & Buchert, S. C. (2021). Characteristics of fragmented aurora-like emissions (FAEs) observed on Svalbard. In *Annales Geophysicae* (Vol. 39, pp. 277–288).
- Emmert, J. T., Drob, D. P., Picone, J. M., Siskind, D. E., Jones, M., Jr., Mlynczak, M., et al. (2021). NRLMSIS 2.0: A whole-atmosphere empirical model of temperature and neutral species densities. *Earth and Space Science*, 8(3), e2020EA001321. https://doi.org/10.1029/2020ea001321
- Emmert, J. T., Jones, M., Jr., Siskind, D. E., Drob, D. P., Picone, J. M., Stevens, M., et al. (2022). NRLMSIS 2.1: An empirical model of nitric oxide incorporated into MSIS. *Journal of Geophysical Research: Space Physics*, 127(10), e2022JA030896. https://doi.org/10.1029/2022ja030896
- Eyler, E., & Pipkin, F. (1983). Lifetime measurements of the  $B^3\Pi_g$  state of  $N_2$  using laser excitation. Journal of Chemical Physics, 79(8), 3654–3659. https://doi.org/10.1063/1.446304
- Farley, D., Jr. (1959). A theory of electrostatic fields in a horizontally stratified ionosphere subject to a vertical magnetic field. *Journal of Geophysical Research*, 64(9), 1225–1233. https://doi.org/10.1029/j2064i009p01225
- Gallardo-Lacourt, B., Frey, H., & Martinis, C. (2021). Proton aurora and optical emissions in the subauroral region. Space Science Reviews, 217, 1–36. https://doi.org/10.1007/s11214-020-00776-6
- Gillies, D. M. (2023). TREx spectrograph observations from Lucky Lake, SK on April 10, 2018 [Dataset]. Gasque. https://data.phys.ucalgary.ca/sort\_by\_project/other/publication\_datasets/Gasque2023/
- Gillies, D. M., Donovan, E., Hampton, D., Liang, J., Connors, M., Nishimura, Y., et al. (2019). First observations from the TREx spectrograph: The optical spectrum of STEVE and the picket fence phenomena. *Geophysical Research Letters*, 46(13), 7207–7213. https://doi.org/10.1029/2019g1083272
- Gillies, D. M., Liang, J., Gallardo-Lacourt, B., & Donovan, E. (2023). New insight into the transition from a SAR arc to STEVE. *Geophysical Research Letters*, 50(6), e2022GL101205. https://doi.org/10.1029/2022g1101205
- Gull, S. F. (1989). Bayesian data analysis: Straight-line fitting. In Maximum entropy and Bayesian methods (pp. 511-518). Springer.
- Gurevich, A. V. (1978). Nonlinear phenomena in the ionosphere. Springer-Verlag.
- Hagelaar, G., & Pitchford, L. C. (2005). Solving the Boltzmann equation to obtain electron transport coefficients and rate coefficients for fluid models. Plasma Sources Science and Technology, 14(4), 722–733. https://doi.org/10.1088/0963-0252/14/4/011
- Hallinan, T., Kimball, J., Stenbaek-Nielsen, H., & Deehr, C. (1997). Spectroscopic evidence for suprathermal electrons in enhanced auroras. *Journal of Geophysical Research*, 102(A4), 7501–7508. https://doi.org/10.1029/97ja00197
- Harding, B. J., Mende, S. B., Triplett, C. C., & Wu, Y.-J. J. (2020). A mechanism for the STEVE continuum emission. Geophysical Research Letters, 47(7), e2020GL087102. https://doi.org/10.1029/2020gl087102
- Ilma, R. (2017). rilma/pyiri2016: Official release of the iri2016 wrapper in python. https://doi.org/10.5281/zenodo.240895
- Itikawa, Y., & Ichimura, A. (1990). Cross sections for collisions of electrons and photons with atomic oxygen. *Journal of Physical and Chemical Reference Data*, 19(3), 637–651. https://doi.org/10.1063/1.555857
- Karlsson, T., & Marklund, G. (1998). Simulations of effects of small-scale auroral current closure in the return current region. *Physics of Space Plasmas*, 15, 401.
- Karlsson, T., Marklund, G., Brenning, N., & Axnäs, I. (2005). On enhanced aurora and low-altitude parallel electric fields. *Physica Scripta*, 72(5), 419–422. https://doi.org/10.1238/physica.regular.072a00419
- Laher, R. R., & Gilmore, F. R. (1990). Updated excitation and ionization cross sections for electron impact on atomic oxygen. *Journal of Physical and Chemical Reference Data*, 19(1), 277–305. https://doi.org/10.1063/1.555872
- Lawton, S., & Phelps, A. (1978). Excitation of the  $b^{-1}\Sigma^{+}_{g}$  state of  $O_{2}$  by low energy electrons. *Journal of Chemical Physics*, 69(3), 1055–1068. https://doi.org/10.1063/1.436700

GASQUE ET AL. 9 of 11

19448007,

- Liang, J., St-Maurice, J., & Donovan, E. (2021). A time-dependent two-dimensional model simulation of lower ionospheric variations under intense SAID. *Journal of Geophysical Research: Space Physics*, 126(12), e2021JA029756. https://doi.org/10.1029/2021ja029756
- Liang, J., Zou, Y., Nishimura, Y., Donovan, E., Spanswick, E., & Conde, M. (2021). Neutral wind dynamics preceding the STEVE occurrence and their possible preconditioning role in STEVE formation. *Journal of Geophysical Research: Space Physics*, 126(3), e2020JA028505. https:// doi.org/10.1029/2020ja028505
- Lucas, G. (2023). pymsis. https://doi.org/10.5281/zenodo.7581692
- Lynch, K. A., McManus, E., Gutow, J., Burleigh, M., & Zettergren, M. (2022). An ionospheric conductance gradient driver for subauroral picket fence visible signatures near STEVE events. *Journal of Geophysical Research: Space Physics*, 127(12), e2022JA030863. https://doi. org/10.1029/2022ja030863
- MacDonald, E. A., Donovan, E., Nishimura, Y., Case, N. A., Gillies, D. M., Gallardo-Lacourt, B., et al. (2018). New science in plain sight: Citizen Scientists lead to the discovery of optical structure in the upper atmosphere. Science Advances, 4(3), eaaq0030. https://doi.org/10.1126/sciadv.aaq0030
- Marklund, G. (1993). Viking investigations of auroral electrodynamical processes. Journal of Geophysical Research, 98(A2), 1691–1704. https://doi.org/10.1029/92ja01518
- Marklund, G., Karlsson, T., & Clemmons, J. (1997). On low-altitude particle acceleration and intense electric fields and their relationship to black aurora. *Journal of Geophysical Research*, 102(A8), 17509–17522. https://doi.org/10.1029/97ja00334
- Martinis, C., Griffin, I., Gallardo-Lacourt, B., Wroten, J., Nishimura, Y., Baumgardner, J., & Knudsen, D. (2022). Rainbow of the night: First direct observation of a SAR arc evolving into STEVE. Geophysical Research Letters, 49(11), e2022GL098511. https://doi.org/10.1029/2022gl098511
- Meier, R. (1991). Ultraviolet spectroscopy and remote sensing of the upper atmosphere. Space Science Reviews, 58(1), 1–185. https://doi.org/10.1007/bf01206000
- Mende, S., Harding, B., & Turner, C. (2019). Subauroral green Steve arcs: Evidence for low-energy excitation. Geophysical Research Letters, 46(24), 14256–14262. https://doi.org/10.1029/2019gl086145
- Michael (2021). space-physics/igrf: Robust build, MATLAB unit test. https://doi.org/10.5281/zenodo.5560949
- Mishin, E., & Streltsov, A. (2022). On the kinetic theory of subauroral arcs. *Journal of Geophysical Research: Space Physics*, 127(8), e2022JA030667. https://doi.org/10.1029/2022ja030667
- Morrill, J., Bucsela, E., Pasko, V., Berg, S., Heavner, M., Moudry, D., et al. (1998). Time resolved N<sub>2</sub> triplet state vibrational populations and emissions associated with red sprites. *Journal of Atmospheric and Solar-Terrestrial Physics*, 60(7–9), 811–829. https://doi.org/10.1016/s1364-6826(98)00031-5
- Nishimura, Y., Dyer, A., Kangas, L., Donovan, E., & Angelopoulos, V. (2023). Unsolved problems in strong thermal emission velocity enhancement (STEVE) and picket fence. Frontiers in Astronomy and Space Sciences, 10, 3. https://doi.org/10.3389/fspas.2023.1087974
- Nishimura, Y., Gallardo-Lacourt, B., Zou, Y., Mishin, E., Knudsen, D., Donovan, E., et al. (2019). Magnetospheric signatures of STEVE: Implications for the magnetospheric energy source and interhemispheric conjugacy. *Geophysical Research Letters*, 46(11), 5637–5644. https://doi.org/10.1029/2019g1082460
- Pancheshnyi, S., Biagi, S., Bordage, M.-C., Hagelaar, G., Morgan, W., Phelps, A., & Pitchford, L. C. (2012). The LXCat project: Electron scattering cross sections and swarm parameters for low temperature plasma modeling. *Chemical Physics*, 398, 148–153. https://doi.org/10.1016/j.chemphys.2011.04.020
- Paschmann, G., Haaland, S., Treumann, R., & Treumann, R. A. (2003). Auroral plasma physics (Vol. 15). Springer Science & Business Media.
  Pfaff, R., Uribe, P., Fourre, R., Kujawski, J., Maynard, N., Acuna, M., et al. (2021). The vector electric field investigation (VEFI) on the C/NOFS satellite. Space Science Reviews, 217(8), 1–88. https://doi.org/10.1007/s11214-021-00859-y
- Phelps, A., & Pitchford, L. (1985). Anisotropic scattering of electrons by N<sub>2</sub> and its effect on electron transport. *Physics Reviews*, 31(5), 2932–2949. https://doi.org/10.1103/physreva.31.2932
- Picone, J., Hedin, A., Drob, D. P., & Aikin, A. (2002). NRLMSISE-00 empirical model of the atmosphere: Statistical comparisons and scientific issues. *Journal of Geophysical Research*, 107(A12), SIA15-1–SIA15-16. https://doi.org/10.1029/2002ja009430
- Raizer, Y. P. (1991). Gas discharge physics. Springer-Verlag.
- Semeter, J., Hunnekuhl, M., MacDonald, E., Hirsch, M., Zeller, N., Chernenkoff, A., & Wang, J. (2020). The mysterious green streaks below STEVE. AGU Advances, 1(4), e2020AV000183. https://doi.org/10.1029/2020av000183
- Shelley, E. (1995). The auroral acceleration region: The world of beams, conies, cavitons, and other plasma exotica. *Reviews of Geophysics*, 33(S1), 709–714. https://doi.org/10.1029/95rg00253
- Shemansky, D. E., & Liu, X. (2005). Evaluation of electron impact excitation of  $N_2$  X  $^1\Sigma_g^{}^+(0)$  into the  $N_2$  + X  $^2\Sigma_g^{}^+(v)$ , A  $^2\Pi_u(v)$ , and B  $^2\Sigma_u^{}^+(v)$  states. Journal of Geophysical Research, 110(A7).
- Vallance Jones, A. (1974). Aurora. D. Reidel publishing company.
- Wardinski, I., Saturnino, D., Amit, H., Chambodut, A., Langlais, B., Mandea, M., & Thebault, E. (2020). Geomagnetic core field models and secular variation forecasts for the 13th International Geomagnetic Reference Field (IGRF-13). Earth Planets and Space, 72(1), 1–22. https://doi.org/10.1186/s40623-020-01254-7
- Yadav, S., Shiokawa, K., Otsuka, Y., Connors, M., & St Maurice, J.-P. (2021). Multi-wavelength imaging observations of STEVE at Athabasca, Canada. *Journal of Geophysical Research: Space Physics*, 126(2), 2020JA028622. https://doi.org/10.1029/2020ja028622
- Yonker, J. D., & Bailey, S. M. (2020). N<sub>2</sub>(A) in the terrestrial thermosphere. *Journal of Geophysical Research: Space Physics*, 125(1), e2019JA026508. https://doi.org/10.1029/2019ja026508

### **References From the Supporting Information**

- Campbell, L., Cartwright, D. C., Brunger, M. J., & Teubner, P. J. O. (2006). Role of electronic excited N<sub>2</sub> in vibrational excitation of the N<sub>2</sub> ground state at high latitudes. *Journal of Geophysical Research*, 111(A9), A09317. https://doi.org/10.1029/2005ja011292
- Eastes, R. W. (2000). Modeling the N<sub>2</sub> Lyman-Birge-Hopfield bands in the dayglow: Including radiative and collisional cascading between the singlet states. *Journal of Geophysical Research*, 105(A8), 18557–18573. https://doi.org/10.1029/1999ja000378
- Grubbs, G., Michell, R., Samara, M., Hampton, D., Hecht, J., Solomon, S., & Jahn, J.-M. (2018). A comparative study of spectral auroral intensity predictions from multiple electron transport models. *Journal of Geophysical Research: Space Physics*, 123(1), 993–1005. https://doi.org/10.1002/2017ja025026
- Liu, N., & Pasko, V. P. (2005). Molecular nitrogen LBH band system far-UV emissions of sprite streamers. *Geophysical Research Letters*, 32(5), L05104. https://doi.org/10.1029/2004gl022001

GASQUE ET AL. 10 of 11



## **Geophysical Research Letters**

10.1029/2023GL106073

Porter, H. S., Jackman, C. H., & Green, A. E. S. (1976). Efficiencies for production of atomic nitrogen and oxygen by relativistic proton impact in air. *Journal of Chemical Physics*, 65(1), 154–167. https://doi.org/10.1063/1.432812

Strickland, D., Bishop, J., Evans, J., Majeed, T., Shen, P., Cox, R., et al. (1999). Atmospheric ultraviolet radiance integrated code (AURIC): Theory, software architecture, inputs, and selected results. *Journal of Quantitative Spectroscopy and Radiative Transfer*, 62(6), 689–742. https://doi.org/10.1016/s0022-4073(98)00098-3

GASQUE ET AL. 11 of 11